

UC Davis

UC Davis Previously Published Works

Title

Structural and functional leaf diversity lead to variability in photosynthetic capacity across a range of *Juglans regia* genotypes

Permalink

<https://escholarship.org/uc/item/6f67z55h>

Journal

Plant Cell & Environment, 45(8)

ISSN

0140-7791

Authors

Momayyezi, Mina
Rippner, Devin A
Duong, Fiona V
et al.

Publication Date




2022-08-01

DOI

10.1111/pce.14370

Peer reviewed

Structural and functional leaf diversity lead to variability in photosynthetic capacity across a range of *Juglans regia* genotypes

Mina Momayyezi¹  | Devin A. Rippner² | Fiona V. Duong¹ | Pranav V. Raja¹ | Patrick J. Brown³ | Daniel A. Kluepfel⁴ | J. Mason Earles¹ | Elisabeth J. Forrestel¹ | Matthew E. Gilbert³  | Andrew J. McElrone^{1,4} 

¹Department of Viticulture and Enology, University of California, Davis, California, USA

²USDA-ARS, Horticultural Crops Research Unit, Prosser, Washington, USA

³Department of Plant Sciences, University of California, Davis, California, USA

⁴USDA-ARS, Crops Pathology and Genetics Research Unit, Davis, California, USA

Correspondence

Mina Momayyezi, Department of Viticulture and Enology, University of California, Davis, CA 95616, USA.

Email: mmomayyezi@ucdavis.edu

Funding information

USDA-ARS CRIS, Grant/Award Number: #5306-21220-004-00; Katherine Esau Postdoctoral Fellowship, UC Davis

Abstract

Similar to other cropping systems, few walnut cultivars are used as scion in commercial production. Germplasm collections can be used to diversify cultivar options and hold potential for improving crop productivity, disease resistance and stress tolerance. In this study, we explored the anatomical and biochemical bases of photosynthetic capacity and response to water stress in 11 *Juglans regia* accessions in the U.S. department of agriculture, agricultural research service (USDA-ARS) National Clonal Germplasm. Net assimilation rate (A_n) differed significantly among accessions and was greater in lower latitudes coincident with higher stomatal and mesophyll conductances, leaf thickness, mesophyll porosity, gas-phase diffusion, leaf nitrogen and lower leaf mass and stomatal density. High CO_2 -saturated assimilation rates led to increases in A_n under diffusional and biochemical limitations. Greater A_n was found in lower-latitude accessions native to climates with more frost-free days, greater precipitation seasonality and lower temperature seasonality. As expected, water stress consistently impaired photosynthesis with the highest % reductions in lower-latitude accessions (A3, A5 and A9), which had the highest A_n under well-watered conditions. However, A_n for A3 and A5 remained among the highest under dehydration. *J. regia* accessions, which have leaf structural traits and biochemistry that enhance photosynthesis, could be used as commercial scions or breeding parents to enhance productivity.

KEYWORDS

CO_2 conductance, leaf anatomy, photosynthesis, walnut wild accessions

This is an open access article under the terms of the Creative Commons Attribution License, which permits use, distribution and reproduction in any medium, provided the original work is properly cited.

© 2022 The Authors. Plant, Cell & Environment published by John Wiley & Sons Ltd.

1 | INTRODUCTION

Common walnut, *Juglans regia* L., is an important and widely grown agronomic species with major production areas concentrated in the northern hemisphere. Its natural range encompasses mountains from western China to central Asia (McGranahan & Leslie, 2009) and was extended by humans spreading the species throughout eastern and southwestern Europe from Central Asia (Leslie & McGranahan, 1998). Throughout its natural habitat, *J. regia* grows under a range of climatic conditions with mean monthly maximum temperatures ranging from -9 to $+30^{\circ}\text{C}$ and annual cumulative precipitation from 175 to 1150 mm during the growing season (Geospatial Data; Duke, 1978; FAO, 2021 [<https://aquastat.fao.org/climate-information-tool/>]; Figure S1). *J. regia* has been utilized to develop commercial scion cultivars (e.g., Chandler) and hybrid rootstocks with resistance to abiotic and biotic stresses (Kluepfel et al. 2015; Leslie, et al. 2015). Global walnut production is highly dependent on the limited genetic diversity of the commonly used scions. For example, only four scion cultivars account for $\sim 80\%$ of total yields. This results in orchard susceptibility to abiotic stresses, disease and pathogens. In California, the Chandler cultivar accounts for 50% of productive acreage (USDA-NASS, 2020) but has limited capacity in dealing with high temperatures and water deficits, which can also increase susceptibility to plant pathogens and low-quality kernel production (Grant & Shackel, 1998; Lampinen et al., 2005; Rosati et al., 2006). Wild germplasm collections can serve as a valuable resource to increase genetic variability to improve tolerance to abiotic and biotic stressors and crop productivity. The diverse *J. regia* collection at the U.S. department of agriculture, agricultural research service (USDA-ARS) National Clonal Germplasm Repository (NCGR) located in Winters, CA, USA, holds such potential. However, to date, this collection has not been exploited to identify genotypes with increased abiotic stress tolerance and physiological traits related to enhanced yield.

Photosynthesis is a key determinant of crop productivity and positively related to biomass accumulation and yield production (Faralli & Lawson, 2020; Fischer et al., 1998; Kruger & Volin, 2006; Long et al. 2006; Simkin et al. 2019). Photosynthetic CO_2 response curves ($A_n - C_i$; net assimilation, A_n vs. CO_2 inside the leaf, C_i) can be used to assess the biochemical and diffusive limitations that determine photosynthetic rates (Long & Bernacchi, 2003; Sharkey 2016). The biochemical limitations are determined from the maximum carboxylation rate of Rubisco (V_{cmax}), the maximum rate of electron transport (J_{max}) and the maximum rate of triose phosphate use (TPU), all derived from $A_n - C_i$ curves. When combined with chlorophyll fluorescence measurements, $A_n - C_i$ curves can also provide information on diffusive limitations associated with mesophyll conductance (g_m ; Harley et al., 1992), which is a measure of the ease with which CO_2 diffuses from the substomatal cavity to the site of carboxylation inside chloroplasts. Recently, these biochemical characteristics have been used to evaluate germplasm in crop breeding programmes (De Souza & Long, 2018; De Souza et al., 2020).

Identifying variation in diffusive limitations which are strongly linked to g_m and leaf structure can also be used in breeding programs

to improve photosynthesis (Tomás et al., 2013; Tosens et al., 2012). g_m involves a complex pathway and a series of resistances in both the gas and liquid phases (Flexas et al., 2008; Tosens & Laanisto, 2018), and is impacted by various leaf structural traits including intercellular airspace (IAS) volume (i.e., porosity), mesophyll surface area exposed to the IAS ($SA_{\text{mes}}/V_{\text{mes}}$), mesophyll cell diameter and density, and cell wall thickness (Evans, 2021; Flexas et al., 2008, 2012; Thérroux-Rancourt & Gilbert, 2017). Leaf structure of some species exhibits plasticity in response to the growth environment (Salk, 2012), resulting in functional variation, which can help optimize resource use (Muir et al., 2017; Wright et al., 2004). Any inherent variation in leaf structural and physiological traits, as a function of the habitat environment to which it has been adapted, may play an important role in regulating photosynthetic capacity in *J. regia* accessions. We also recently found that two *Juglans* spp. exhibit changes in mesophyll structure under dehydration associated with changes in cell volume, orientation and arrangement that increases porosity (Momayyezi et al., 2022). Desiccation influences CO_2 diffusion and water relations as mesophyll cell turgor changes (Buckley et al., 2017; Scoffoni et al., 2014). How genotypic diversity in mesophyll cell packing and distribution across *J. regia* accessions may link with photosynthetic performance and susceptibility to drought is yet to be investigated. X-ray microcomputed tomography (microCT) provides an in-depth assessment of leaf mesophyll traits (i.e., porosity and tortuosity) and cells orientation and geometry (Earles et al., 2018, 2019; Lundgren & Fleming, 2020; Thérroux-Rancourt et al., 2020).

In this study, we combined gas exchange physiological analysis with microCT imaging of leaves to explore: (1) the photosynthetic capacity of numerous *J. regia* wild accessions originating from habitats with varied climatic conditions; (2) links between leaf structural diversity and physiological features that enhance photosynthetic capacity; and (3) whether genotypic differences hold up under water stress conditions. Based on our previous observations for two *Juglans* species (Momayyezi et al. 2022), we hypothesize that greater A_n will be associated with thicker leaves and higher mesophyll porosity and gas-phase diffusion (g_{IAS} ; Han et al., 2019; Tomás et al., 2013). We also expect accessions originating from lower latitudes, characterized by warmer and wetter habitats, would exhibit higher inherent A_n to support growth through enhanced biochemical activities as predicted for plants under warmer conditions (Moore et al., 2021; Ruiz-Vera et al., 2018). We anticipate that greater A_n would be concurrent with higher IAS and conductance as temperature and precipitation are known to strongly influence functional diversity of photosynthesis across species (Harrison et al., 2020; Ordonez & Svenning, 2017).

2 | MATERIALS AND METHODS

Stems were collected from 11 genetically unique *J. regia* accessions (Figure 1a,b) at the USDA-ARS-NCGR in Wolfskill Experimental Orchard, Winters, CA, USA, to use as scion and were grafted by

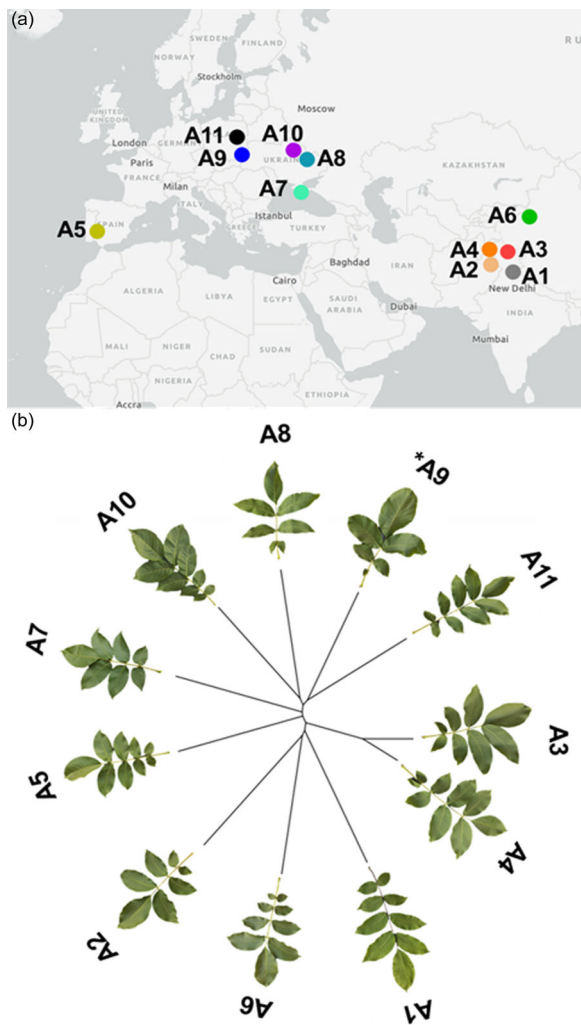


FIGURE 1 (a) Geographic distribution map for 11 *J. regia* accessions. Location data were found in the USDA-ARS National Plant Germplasm System for individual accessions (Germplasm Resources Information Network, GRIN). (b) Unrooted neighbour-joining tree for 11 *J. regia* accessions. Thirteen thousand three hundred and twenty polymorphic single nucleotide polymorphisms (SNPs) among these 11 trees were discovered by Illumina sequencing for the tip leaflet and used to construct NJ trees in R using the “phangorn” package. *Genotype data from C4 29, different individual but same accession as A9 (C4 28; see Table S1) was used, as data for original A9 was not available.

Sierra Gold Nursery onto a commonly used commercial rootstock, RX1 (*Juglans microcarpa* × *J. regia*). We used a common rootstock to eliminate any own-root effects and to simulate conditions for a commercial walnut orchard setting, where rootstocks are commonly used. The grafted saplings were repotted and transferred to the Armstrong lathe house facility at the University of California, Davis, in June 2019, and kept under natural light, temperature and relative humidity (~50%). The budburst for accessions occurred between April and May.

Measurements were initiated on nonstressed plants in August 2019 under well-watered conditions for all accessions. The measurements on the same plants were repeated under dehydrated condition through a gradual dry down procedure using the methods as described by Knipfer et al. (2020). Briefly, water loss from pots via transpiration and soil evaporation were quantified during the experiment by weighing pots to calculate the required amount of water needed per pot under each treatment, daily. After completion of measurements in nonstressed conditions, water application was reduced to 75% of full irrigation during the first week and then to 50% of full irrigation in the second week of drying. This watering regime was then maintained for the dehydration treatment until completion of the experiment. Plants were maintained under ambient natural light with a ~15 h photoperiod during the experiment, maximum temperature of 35°C during day and minimum of 15°C during night, in 2.65 L pots containing a 40% pine bark, 40% sphagnum peat moss and 20% vermiculite, and a thin layer of the slow-release fertilizer (Osmocote Smart-Release Plus) was added to the top soil at the plantation time. The two irrigation treatments were maintained for ~2 weeks before the measurements.

2.1 | Illumina sequencing and phylogeny tree construction

Genotyping-by-sequencing libraries were prepared by restricting genomic DNA with HindIII-HF (NEB) with Ampure XP bead (Beckman-Coulter) cleanup. Sequence data were obtained on an Illumina HiSeq 4000 instrument at the UC Davis Genome Center. Single nucleotide polymorphism (SNP) calling was performed using the TASSEL GBS pipeline (Glaubitz et al., 2014) with alignment to the Chandler genome (Marrano et al., 2020), resulting in 13,320 polymorphic SNPs. The phangorn package in R (R Core Team, 2017; Schliep et al., 2017) was used to construct a neighbour-joining tree from the distance matrix.

2.2 | Photosynthetic measurements

Net assimilation rate (A_n), stomatal conductance (g_s) and the IAS CO_2 concentration (C_i) were measured on one leaflet of the leaf from each accession in five replications using a LI-COR 6800 system fitted with 6800-01A fluorometer. To provide a general leaf developmental assessment before the measurements, the leaf plastochrone index (LPI) was calculated as described by Erickson & Michelini (1957). The 4th or 5th leaflet was counted down from the tip leaflet on the leaves at LPI between 5 and 6. All measurements were done under photosynthetic photon flux density (PPFD) of $1500 \mu\text{mol m}^{-2} \text{s}^{-1}$ (10% blue vs. 90% red), a saturating PPFD for all accessions (Figure S2), chamber temperature at 25°C, ambient chamber CO_2 concentration (C_a) at $400 (\mu\text{mol mol}^{-1})$, flow rate at $500 (\mu\text{mol air s}^{-1})$ and vapour pressure deficit between 1.5 and 2.0 kPa. To calculate the

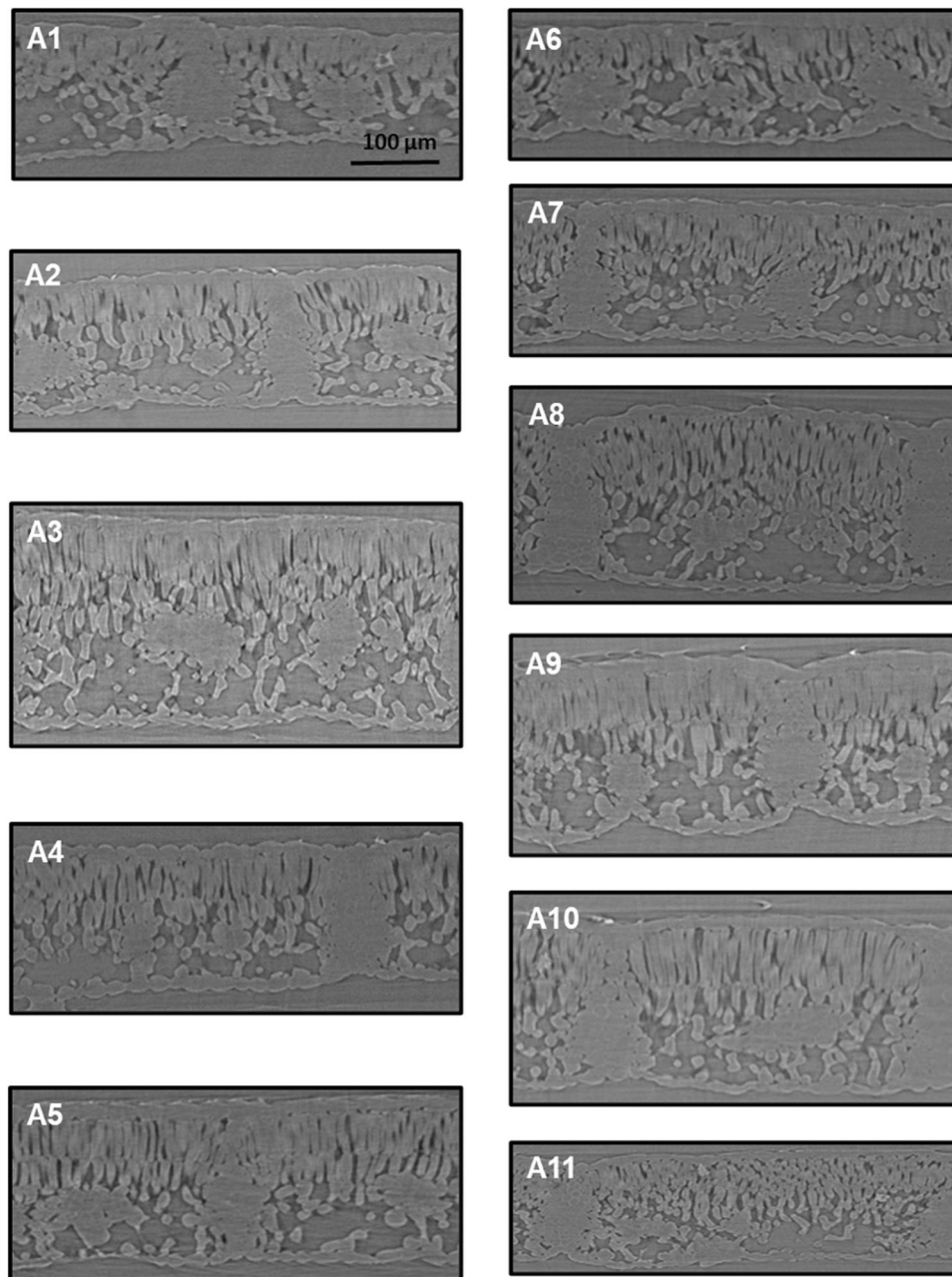


FIGURE 2 Leaf cross sections from representative scans for 11 *J. regia* accessions under well-watered condition obtained using X-ray microcomputed tomography.

intrinsic water use efficiency (WUE_i), A_n was divided by g_s for each accession in five replications under both well-watered and dehydrated conditions. The 6 cm² round fluorometer gasket set was filled fully with the leaflet area and was changed frequently between the measurements, along with running corrections suggested by the manufacturer to reduce errors of CO₂ and H₂O leakage through the gasket. To obtain the maximum quantum yield of photosystem II, all leaflets were dark adapted for 20 min before all other measurements. The quantum yield of photosystem II (Φ_{PSII}) under actinic light was obtained by application of saturating multiphase flashes (>8000 $\mu\text{mol m}^{-2} \text{s}^{-1}$) as in Genty et al. (1989).

2.3 | Calculation of g_m by chlorophyll fluorescence and of CO₂ concentration in the chloroplast (C_c)

The “variable J method” was used to estimate g_m based on calculation of electron transport rate (J_{flu}) from measurements of chlorophyll fluorescence (Bongi & Loreto, 1989; Harley et al., 1992):

$$J_{flu} = \Phi_{PSII} \times \text{PPFD} \times \alpha \times \beta \quad (1)$$

where β (0.5 for C₃ plants) is the fraction of absorbed quanta reaching photosystem II (Bernacchi et al., 2002). The leaf absorbance, α , was previously measured for *Juglans* species to be 85.3% based on the

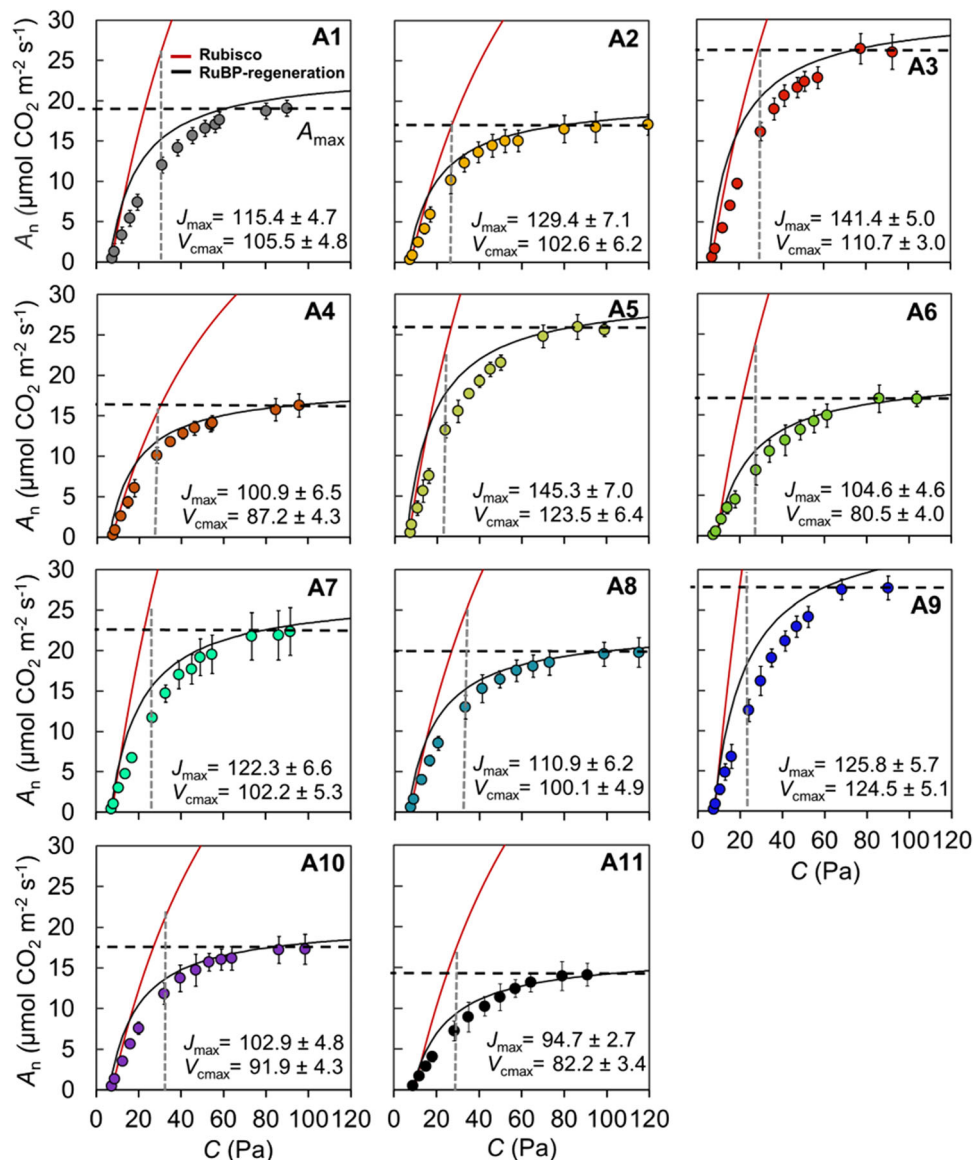


FIGURE 3 Photosynthetic CO₂ response curves were constructed using Sharkey's fitting calculator version 2.0 (Sharkey 2016), averaged for 5 replications in 11 *J. regia* accessions under well-watered condition. A - C_i curves are shown with coloured circles and error bars measured directly. A - C_c curves were used to generate V_{cmax} and J_{max}, and averaged over five replications for each accession (±SE, n = 5). Black dashed horizontal line indicates assimilation rate at saturating CO₂ (A_{max}) at triose phosphate use (TPU) limitation state, and Rubisco and RuBP regeneration limitations are indicated for each accession by red and black curves, respectively. Colour scheme is consistent with accession numbers presented in Figure 3 and in Table 1. Dashed vertical grey lines on each plot represent the C_i at ambient CO₂ of 40.4 Pa, which represents the limitation of g_m in comparison with the value of the A - C_c curve (i.e., the point where C_i and C_c would be equal). [Color figure can be viewed at wileyonlinelibrary.com]

average value (±0.2 SE) in all individuals using an ASD Fieldspec spectroradiometer (ViewSpec Pro, ASD Inc.; Momayyezi et al., 2022). g_m was given by (Harley et al., 1992):

$$g_m = A_n / \left[C_i - \left(\frac{\Gamma^*(J_{\text{flu}} + 8(A_n + R_d))}{J_{\text{flu}} - 4(A_n + R_d)} \right) \right] \quad (2)$$

where R_d is the nonphotorespiratory respiration rate in the light and Γ* is the chloroplast CO₂ photocompensation point. Γ* was assumed to equal

the intercellular CO₂ photocompensation point (C_i^{*}) per Gilbert et al. (2012). We used previously reported R_d ± SE (0.73 ± 0.08 μmol m⁻² s⁻¹) and C_i^{*} ± SE (38.18 ± 0.47 μmol mol⁻¹), which were found using the Laisk method (Laisk, 1977, in Gilbert et al., 2012) as the point of intersection of the linear portion of averaged four sets of A_n - C_i curves obtained at three irradiances (100, 200 and 500 μmol m⁻² s⁻¹) and 13 CO₂ concentrations (35, 40, 50, 60, 70, 80, 90, 100, 110, 120, 140, 160 and 180 μmol mol⁻¹). We used this approach previously for two *Juglans* species with contrasting leaf anatomy (Momayyezi et al., 2022) and applied it to the

11 *J. regia* accessions in this study. We assumed any potential small changes in C_i^* and R_d under dehydration will be negligible, and the same values measured for *Juglans* species under well-watered conditions were used to estimate g_m under dehydration. Having obtained g_m by the chlorophyll fluorescence method, the CO_2 concentration in the chloroplast (C_c) was found according to Harley et al. (1992):

$$C_c = C_i - \frac{A_n}{g_m} \quad (3)$$

2.4 | $A_n - C_i$ curves

To better understand photosynthetic responses, we constructed CO_2 response ($A_n - C_i$) curves for each accession using five replications at saturating PPFD ($1500 \mu\text{mol m}^{-2} \text{s}^{-1}$) under the following sample CO_2 concentration: 400, 50, 80, 100, 150, 200, 400, 600, 800, 1000, 1200, 1500 p.p.m. under well-watered and dehydrated conditions. Before running $A_n - C_i$ curves, the seal of the fluorometer chamber was tested for CO_2 leakage by running a full curve at different C_a concentration in empty cuvette and the measurements were corrected using the Licor's equation (Bernacchi et al., 2002; Flexas et al., 2007). The A_n and corresponding C_i values for each accession in five replications were introduced to the Sharkey's fitting calculator version 2.0 (Sharkey 2016), a Farquhar-von Caemmerer-Berry-based model to estimate V_{cmax} , J_{max} and g_m using differences in CO_2 partial pressure between C_i and C_c and predict assimilation rates (A) at the limiting states of Rubisco, RuBP-regeneration and TPU (Sharkey et al., 2007). We used photosynthesis at the TPU state to set the maximum assimilation rate (A_{max}) at saturating CO_2 as in Sharkey et al. (2007). g_m obtained from the chlorophyll fluorescence method was verified against g_m found using $A_n - C_i$ method (Figure S3). g_m obtained from the chlorophyll fluorescence method was used to present correlations, prepare figures and tables and make statistical comparisons for each accession under both well-watered and dehydrated conditions.

2.5 | Leaflet water potentials

Leaflet water potential (Ψ_{leaflet}) was measured using a pressure chamber (PMS Instrument Company, Model 1505D) immediately after gas exchange measurements between 10 AM to 12 PM (Williams & Araujo, 2002). A leaflet directly opposite the one used for gas-exchange measurements was used to measure leaflet water potential from each accession at five replications. Each leaflet was cut at petiolule base and bagged for 10–15 min to allow equilibration within the leaflet. Then, the petiolule was placed inside the pressure chamber gasket. Chamber pressure was increased slowly until the balancing pressure was reached.

2.6 | Leaf mass and nitrogen content per area

Immediately after gas-exchange measurements, the leaflet adjacent to the one used for gas exchange was punched and collected discs

were dried at 72°C oven for 48 h. Using the leaflet discs area and dry weight, leaf mass per area (LMA) was calculated for each accession using five replications. Later, the dried samples were ground and 4.5–5.0 mg of them were encapsulated in tin cups and sent to the Stable Isotope Facility, at University of California Davis for total nitrogen content elemental analysis. Using LMA data, the nitrogen content results per unit mass were converted to leaf nitrogen content per unit area (Leaf N).

2.7 | X-ray microCT imaging

Leaves from each accession and treatment in five replications were scanned using X-ray microCT at beamline 8.3.2 at the Advanced Light Source (ALS) in Lawrence Berkeley National Laboratory, Berkeley, CA, USA. The same leaflet samples used for gas exchange were collected from the plants, bagged and placed in a cooler at room temperature an hour before scanning in ALS. Leaves from the well-watered conditions were collected and scanned in September 2019. After the plants went through the dehydration process, leaves were similarly collected and scanned at ALS in October 2019. A single piece of 3 mm-wide and 7 mm-long was taken from middle of the leaflet lamina from each plant and enclosed between two pieces of Kapton tape to prevent desiccation of the tissue and sample movement during the scanning. Samples were placed inside the end of a pipette tip and scanned under a continuous tomography mode at 23 keV using $\times 10$ objective lens with a pixel resolution of $0.65 \mu\text{m}$. Raw tomographic data were reconstructed using TomoPy (Gürsoy et al., 2014) through both gridrec and phase-retrieval reconstruction (Davis et al., 1995; Dowd et al., 1999).

2.8 | Mesophyll surface area, porosity, tortuosity and lateral path lengthening

Mesophyll porosity, θ_{IAS} ($\text{m}^3 \text{m}^{-3}$) was calculated as the IAS volume as a fraction of the total mesophyll volume as described by Th eroux-Rancourt et al. (2017). The IAS volume (V_{IAS}) to mesophyll cell volume ($V_{\text{mes-cell}}$) ratio and the mesophyll surface area exposed to the IAS (SA_{mes}) per mesophyll volume (V_{mes}) were calculated as $V_{\text{IAS}}/V_{\text{mes-cell}}$ ($\text{m}^3 \text{m}^{-3}$) and $SA_{\text{mes}}/V_{\text{mes}}$ ($\mu\text{m}^2 \mu\text{m}^{-3}$), respectively.

The tortuosity factor, τ ($\text{m}^2 \text{m}^{-2}$), was the diffusive path length within the IAS (i.e., the actual path from the stomate to a cell surface; geodesic distance [L_{geo}]) to the straight path length without any physical obstacles to diffusion between the stomate and the cell surface (Euclidean distance, L_{Euc}):

$$\tau = \left(\frac{L_{\text{geo}}}{L_{\text{Euc}}} \right)^2 \quad (4)$$

as described in Earles et al., (2018). The L_{geo} and L_{Euc} were mapped and quantified for all voxels along the mesophyll surface and τ was calculated for the whole three-dimensional (3D) image array as in

Earles et al. (2018). Then, leaf-level tortuosity (τ_{leaf}) was calculated as the mean of τ values at the edge of mesophyll cells. The lateral path lengthening λ (m m^{-1}) was calculated using L_{Euc} and a second distance map as described by Earles et al. (2018) to measure the shortest unobstructed distance in a straight line between the abaxial epidermis and all points along the mesophyll surface L_{epi} (Legland et al., 2016):

$$\lambda = \frac{L_{\text{Euc}}}{L_{\text{epi}}} \quad (5)$$

Similarly, leaf-level lateral path lengthening (λ_{leaf}) was then calculated as the mean of λ values at the edge of mesophyll cells.

Vein volume relative to the leaf volume ratio ($V_{\text{vein}}/V_{\text{leaf}}$, $\text{m}^3 \text{m}^{-3}$) was calculated as a fraction of total leaf volume as described by Trueba et al. (2022) from the same scans used for θ_{IAS} , τ and λ_{leaf} calculations.

2.9 | IAS conductance and stomatal density

The τ_{leaf} , λ_{leaf} and θ_{IAS} were used to calculate leaf-level IAS conductance (g_{IAS}), where D_m is the diffusivity of CO_2 in air ($\text{m}^2 \text{s}^{-1}$). Diffusion path length in gas phase was equal to half of the mesophyll thickness (L_{mes}) for hypostomatous leaves (Earles et al., 2018; Niinemets & Reichstein, 2003; Tomás et al., 2013):

$$g_{\text{IAS}} = \frac{\theta_{\text{IAS}} D_m}{0.5 L_{\text{mes}} \tau_{\text{leaf}} \lambda_{\text{leaf}}} \quad (6)$$

To verify autosegmentation and IAS trait estimation by random forest model, a PyTorch implementation of a fully convolutional network model with a ResNet-101 backbone was used for the semantic segmentation of the leaf image data with cloud-based resources in Google Colab. For training, we used a binary cross-entropy loss function, an Adam optimizer for stochastic optimization with a learning rate of 0.001, a scaling factor of 1 to avoid small feature loss in the training images and a batch size of 1 to accommodate the GPU limitations in Google Colab. Output results were comparable to those generated on the same image sets with a workflow developed by Thérroux-Rancourt et al. (2020) using a random forest model for semantic segmentation of leaf tissues. The output was used to validate tissue surface area and volume determination and 3D leaf projection (Figure S4).

To quantify the stomatal density, the grid reconstructions were used at the paradermal direction. The stomata density and size were measured in 0.04 mm^2 of leaflet area for all accessions ($n = 5$).

2.10 | Climatic data for accessions' native habitats

Coordinates for each accession's native habitats were extracted from the USDA-ARS Germplasm Resources Information Network database (<https://npgsweb.ars-grin.gov/gringlobal/search>). Temperature and precipitation data were obtained from FAO climate information tools

(<https://aquastat.fao.org/climate-information-tool/>) for each of these native habitat locations (Figure S1). The temperature and precipitation seasonality were calculated based on the ratio of the SD for monthly mean temperature or precipitation to the monthly mean temperature or precipitation (known as the coefficient of variation) and multiplied by 100. The temperature or precipitation values for each month were averaged and the SD was calculated using the mean of the 12 months (Donnell & Ignizio, 2012).

2.11 | Statistics

Linear regression and Pearson correlation coefficients were used to examine relationships between latitude, temperature and precipitation seasonality, frost-free days and A_n , A_{max} , g_s , g_m , g_{IAS} , L_{leaf} , θ_{IAS} , λ_{leaf} , τ , $V_{\text{vein}}/V_{\text{leaf}}$, WUE_i , Leaf N, LMA, J_{max} , V_{cmax} and Ψ_{leaflet} using GraphPad prism 9 software (GraphPad Software, Inc.). Paired t -test was used to check for systematic differences between the chlorophyll fluorescence and $A_n - C_i$ curve methods for estimating g_m and C_c . Mixed linear models were used to compare relative changes in percent for A_n , g_m , g_s , L_{leaf} , g_{IAS} , θ_{IAS} and Ψ_{leaflet} under dehydration for all accessions using SAS 9.4 (SAS Institute Inc., 2013). The p required for significance (0.002) was adjusted by dividing α (0.05) by the number of comparisons per test (25 here). Logarithm or squared transformations were performed to meet normality and equal variance assumptions where needed.

3 | RESULTS

Inherent differences in photosynthetic capacity were found among the accessions; *J. regia* accessions 3, 5 and 9 showed the highest photosynthetic capacity, as measured by A_{max} (26.3, 25.6, 27.5 $\mu\text{mol CO}_2 \text{ m}^{-2} \text{ s}^{-1}$, respectively). Higher A_{max} in these accessions was linked to greater maximum carboxylation rate (V_{cmax} , $R^2 = 0.81$, $p < 0.001$) and maximum electron transport rate (J_{max} , $R^2 = 0.67$, $p = 0.002$; Figure 3 and S6). Leaves with higher A_{max} had thicker leaves (L_{leaf} , $p = 0.013$) with greater mesophyll porosity (θ_{IAS} , $p = 0.049$) and leaf nitrogen (Leaf N, $p = 0.044$; Figure S6).

Similarly, A_n was extracted from $A_n - C_i$ curves at C_a of 40.4 (Pa) and was positively correlated with chlorophyll fluorescence g_m ($p < 0.0001$) and g_s ($p = 0.034$; Figure 4) across the accessions. Similar to A_{max} , leaves with greater A_n had thicker leaves (L_{leaf} , $p = 0.037$) and mesophyll (L_{mes} , $p = 0.05$; data not presented), higher mesophyll porosity (θ_{IAS} , $p = 0.041$) and nitrogen content per unit area (Leaf N, $p = 0.012$) but less leaf mass per unit area (LMA, $p = 0.007$; Figure 4). Increased A_n was not significantly related with lateral path lengthening (λ_{leaf} , $p = 0.091$) nor tortuosity (τ_{leaf} , $p > 0.1$; data not presented). Leaves with greater g_m exhibited greater θ_{IAS} ($R^2 = 0.42$; $p = 0.030$), higher mesophyll thickness ($p = 0.034$) and had lower λ_{leaf} ($p = 0.031$; Figure S7). High-porosity leaves had lower $V_{\text{vein}}/V_{\text{leaf}}$ ($p = 0.049$) and WUE_i ($p = 0.047$; Figure S7), and exhibited greater g_s ($p = 0.0003$), concurrent with lower stomatal density ($R^2 = 0.38$; $p = 0.042$). Across accessions, leaflet water potential

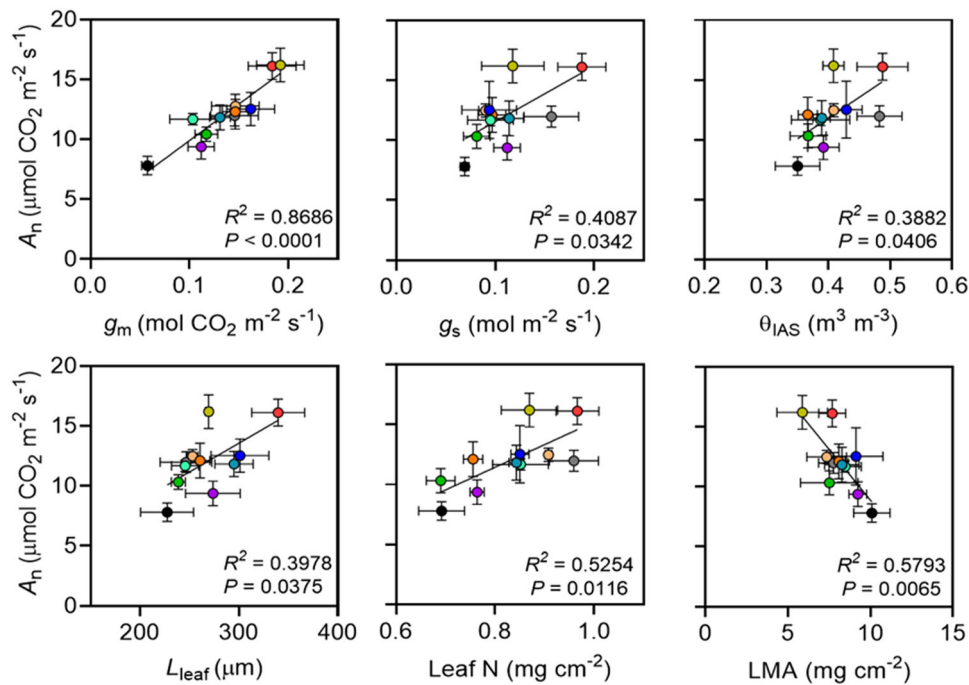


FIGURE 4 Net assimilation rate (A_n , $\mu\text{mol CO}_2 \text{ m}^{-2} \text{ s}^{-1}$) relationship with mesophyll conductance obtained from chlorophyll fluorescence method (g_m , $\text{mol CO}_2 \text{ m}^{-2} \text{ s}^{-1}$), stomatal conductance (g_s , $\text{mol m}^{-2} \text{ s}^{-1}$), mesophyll porosity (θ_{IAS} , $\text{m}^3 \text{ m}^{-3}$), leaf thickness (L_{leaf} , μm), leaf nitrogen per unit area (Leaf N, mg cm^{-2}) and leaf mass per unit area (LMA, mg cm^{-2}) in 11 *J. regia* accessions using mean values ($\pm\text{SE}$, $n = 5$). A_n was extracted from $A_n - C_i$ curves at C_a of 40.4 Pa. Colour scheme is consistent with accession numbers presented in Figure 3 and in Table 1. [Color figure can be viewed at wileyonlinelibrary.com]

($\Psi_{leaflet}$) was positively related to both θ_{IAS} ($p = 0.024$) and g_s ($p = 0.028$).

3.1 | Climate-driven photosynthetic capacity

Photosynthetic capacity and associated leaf physiological and anatomical characteristics for the accessions were associated with the climatic conditions in native habitats. Accessions from habitats with lower temperature seasonality in lower latitudes had higher g_{ias} and Leaf N ($p \leq 0.05$), which may support higher their A_n through greater g_m and θ_{IAS} (Figure 5; $p = 0.05$; Figure S5). Despite nonsignificant relationships, parallel decreases in g_m , g_{IAS} , Leaf N and θ_{IAS} ($p > 0.05$; Figure S5) may suggest a pattern for decline in mesophyll CO_2 diffusion rate with latitude, while they accumulate more LMA ($p = 0.015$; Figure 5). Higher variability in precipitation seasonality and more frost-free days were significantly related to increased g_{IAS} concurrent with lower stomatal density (Figure 5). Decreases in LMA and frost-free days were associated with increases in Leaf N (Figure 5).

3.2 | Responses under dehydration

As expected, dehydration impaired photosynthesis and altered leaf structure with reduced g_s , g_m and L_{leaf} and increased θ_{IAS} and g_{IAS} in

all accessions. The percent reduction in A_n was significantly correlated with percent reductions in g_s ($p = 0.007$), g_m ($p = 0.002$) and $\Psi_{leaflet}$ ($p = 0.002$) under dehydration (Table 1). Accessions A3, A5 and A9, which had the highest A_n and A_{max} under well-watered conditions, exhibited the greatest percent reductions amongst accessions in these parameters under drought stress (i.e., >50% reduction for all 3; Table 1). However, the absolute values of A_n for accessions A3 and A5 were not significantly lower than other accessions under dehydration, whereas they were among the lowest for A9 under dehydration (Table S2). The reduction in L_{leaf} was linked with decreases in g_{ias} ($p = 0.02$) and g_m ($p = 0.08$). The concurrent reduction in $\Psi_{leaflet}$ was significantly correlated with percent decline in g_s ($p = 0.004$; Table 1). Under dehydration, absolute A_n , g_m , θ_{IAS} , g_{IAS} and Leaf N remained negatively correlated with latitude ($p < .05$, Table 2).

4 | DISCUSSION

4.1 | Photosynthetic capacity, mesophyll anatomy, and CO_2 diffusion

Diverse accessions of *J. regia*, native to various habitats with different temperature and precipitation patterns, exhibited variable photosynthetic capacity. Three accessions (A3, A5 and A9) exhibited

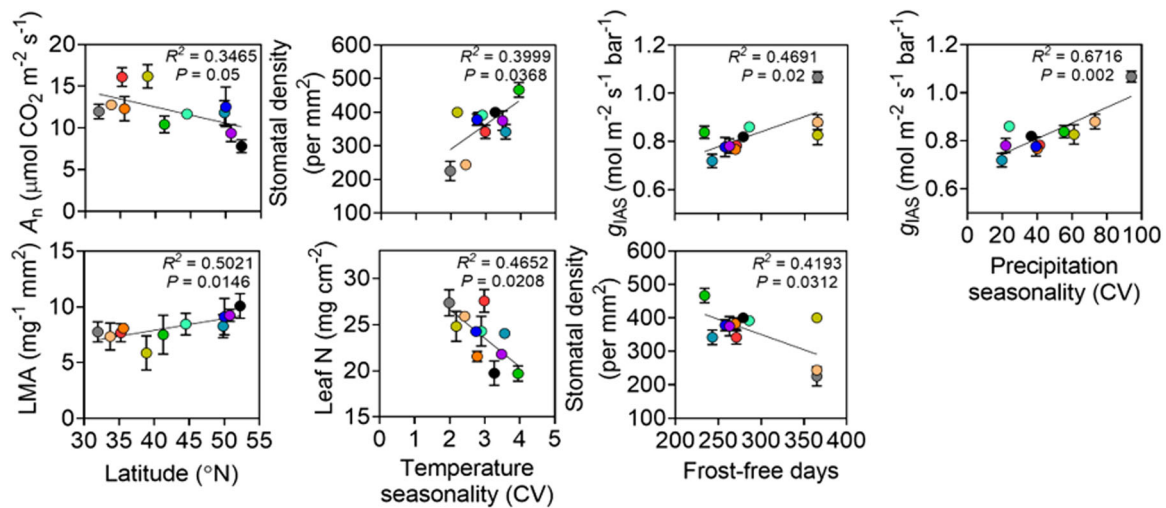


FIGURE 5 Relationship between net assimilation rate (A_n , $\mu\text{mol CO}_2 \text{ m}^{-2} \text{ s}^{-1}$), intercellular airspace (IAS) conductance (g_{IAS} , $\text{mol O}_2 \text{ m}^{-2} \text{ s}^{-1} \text{ bar}^{-1}$), stomatal density (mm^{-2}), leaf mass per unit area (LMA, mg cm^{-2}) and leaf nitrogen per unit area (Leaf N, mg cm^{-2}) using mean values ($\pm \text{SE}$, $n = 5$) and latitude ($^{\circ}\text{N}$), temperature seasonality (coefficient of variation [CV]), precipitation seasonality (CV), and frost-free days in habitats for 11 *J. regia* accessions (see Figure S5 for the full trait correlations). [Color figure can be viewed at wileyonlinelibrary.com]

significantly higher A_n , A_{max} and CO_2 diffusion capacity under the well-watered condition with the highest V_{cmax} and J_{max} . Greater photosynthetic capacity is typically linked to carboxylation capacity via increased Rubisco protein abundance and activity (Hikosaka & Shigeno, 2009; von Caemmerer & Farquhar, 1981; Kattge et al., 2011).

Higher photosynthetic capacity was strongly linked to leaf thickness and mesophyll structure and supported by higher Leaf N. As expected, *J. regia* accessions with higher A_n had thicker leaves and exhibited greater θ_{IAS} and g_m (Figure 4). This agrees with previous findings for *J. regia* cv. Chandler (Momayyezi et al., 2022). *J. regia* accessions with higher A_n had greater A_{max} , V_{cmax} and Leaf N, suggesting higher carboxylation capacity and performance (Figures 3 and S6). Although previous work reported a positive relationship between A_n with LMA (i.e. across *Quercus ilex* provenances; Peguero-Pina et al., 2017), we found *J. regia* accessions exhibited greater A_n with lower LMA. Increasing cell density would reduce mesophyll surface area exposed to IAS as a result of high cell packing and could also be impacted by cell wall thickness (Niinemets et al., 2009a; Tomás et al., 2013; Tosens et al., 2012). A more porous mesophyll and thicker leaves with shorter λ_{leaf} (Figure S7), contributed to higher A_{max} across *J. regia* accessions (Figure S6), highlighting the fact that thickness and cell density may not change in the same direction (Niinemets, 1999; Syvertsen et al., 1995). Increases in leaf porosity are known to reduce diffusive resistance and lateral path lengthening in other species (Earles et al., 2018). Additionally, leaf mesophyll geometry and IAS are known to impact stomatal patterning, photosynthetic capacity and conductances (Baillie & Fleming 2020; Lehmeier et al., 2017; Lundgren et al., 2019); *J. regia* accessions with greater porosity had fewer but larger stomata with significantly greater g_s .

Leaf anatomy also plays an important role in biophysical coordination between CO_2 diffusion and leaf hydraulics (Boyce et al., 2009; Lehmeier et al., 2017; Fulton et al., 2017). Similar to

findings from Trueba et al. (2022), *J. regia* accessions with greater porosity had less $V_{\text{vein}}/V_{\text{leaf}}$ and lower WUE_i (Figure S7) associated with higher g_s . More extensive vasculature, including greater bundle sheath extensions, may improve WUE_i by improving connections between the vascular tissue and epidermis for stomatal regulation and water supply to replace losses due to transpiration (Brodribb et al., 2007; Zwieniecki et al., 2007).

4.2 | Climatic variables and inherent functional diversity

We found that inherent differences in the photosynthetic activity of *J. regia* accessions is associated with climatic conditions in their native habitat (Figures 5 and S5). Other studies have shown that leaf structure and function are strongly related to the environment of a species' native habitat (Li et al., 2018; Reich 2014). Higher precipitation seasonality, concurrent with more frost-free days in lower latitudes, was associated with higher A_n through increased g_m and g_{IAS} . This can be due to increased allocation of Leaf N toward the dynamic biochemical activity rather than more static aspects of the mesophyll (e.g., wall thickness and mesophyll surface area; Evans, 2021; Terashima et al., 2006; Tosens et al., 2012). As discussed by He et al. (2018a), changes in leaf anatomy (i.e., leaf and epidermis thickness, and the ratio of spongy to palisade mesophyll) as a function of latitude are mainly driven by variability in precipitation and temperature. *J. regia* accessions from habitats from lower latitudes with warmer growing season and lower temperature seasonality had leaves with greater g_{IAS} and tortuosity. Greater precipitation during the warmest annual quarter (between June and August), when *J. regia* has the highest water demand for growth and fruit development, was associated with increased g_{IAS} ($p = 0.02$) and reduced SD ($p < 0.001$),

TABLE 1 Percent change in physiological and anatomical variables under dehydration relative to the well-watered condition

Accession #	A_n	g_s	g_m	Ψ_{leaflet}	L_{leaf}	θ_{IAS}	g_{IAS}
A 1	-20.8 ± 0.8 (A2,3,4,5,6,8,9,10,11)	-26.0 ± 3.4 (A2,3,4,5,9,10,11)	-36.4 ± 2.4 (A2,3,4,5,6,7,8,9,10,11)	-39.8 ± 2.7 (A3,5,9)	-8.9 ± 0.8 n.s.	+8.4 ± 1.9 (A3)	+16.5 ± 2.2 (A2,3,6,9)
A 2	-36.2 ± 0.8 (A1,3,5,7,9,10)	-58.3 ± 0.8 (A1,4,6,7,8,9,11)	-53.4 ± 1.9 (A1,5,7)	-49.4 ± 2.3 (A3)	-11.7 ± 1.2 n.s.	+17.0 ± 1.9 (A8,10)	+33.3 ± 1.4 (A1,4,7,8,10,11)
A 3	-50.8 ± 1.6 (A1,2,4,6,7,8)	-66.8 ± 2.1 (A1,4,6,7,8,11)	-54.1 ± 2.6 (A1,5,7)	-66.5 ± 3.8 (A1,2,4,6,7,8,11)	-9.1 ± 0.9 n.s.	+21.8 ± 2.6 (A1,5,6,7,8,10,11)	+35.4 ± 2.5 (A1,4,7,8,10,11)
A 4	-36.9 ± 1.1 (A1,3,5,7,9,10)	-44.5 ± 1.1 (A1,2,3,5,6,7,8,9,10,11)	-61.1 ± 1.9 (A1,5,7,11)	-37.8 ± 3.3 (A3,5,9,10)	-7.6 ± 0.8 (A6)	+15.2 ± 1.1 (A8,10)	+21.6 ± 1.9 (A2,3)
A 5	-56.7 ± 2.2 (A1,2,4,6,7,8,10,11)	-66.7 ± 1.8 (A1,4,6,7,8)	-77.5 ± 2.5 (A1,2,3,4,6,7,8,9,10,11)	-60.9 ± 3.6 (A1,4,6,7,8)	-11.5 ± 1.2 n.s.	+11.3 ± 1.2 (A3)	+24.8 ± 2.1 (A7,10)
A 6	-35.6 ± 0.8 (A1,3,5,7,9,10)	-34.6 ± 0.9 (A2,3,4,5,7,9,10,11)	-60.7 ± 0.7 (A1,5,7,11)	-41.3 ± 2.6 (A3,5,9)	-13.0 ± 1.1 (A4,7,10)	+12.4 ± 2.8 (A3)	+31.2 ± 3.2 (A1,7,10,11)
A 7	-19.9 ± 1.1 (A2,3,4,5,6,8,9,10,11)	-22.3 ± 2.3 (A2,3,4,5,6,8,9,10,11)	-20.2 ± 2.6 (A1,2,3,4,5,6,8,9,10,11)	-39.7 ± 4.6 (A3,5,9)	-6.9 ± 0.9 (A6)	+10.7 ± 1.5 (A3)	+13.2 ± 1.1 (A2,3,5,6,9)
A 8	-40.7 ± 1.5 (A1,3,5,7,9)	-32.1 ± 1.6 (A2,3,4,5,7,9,10,11)	-57.8 ± 1.2 (A1,5,7)	-40.6 ± 2.8 (A3,5,9)	-9.3 ± 0.9 n.s.	+5.6 ± 1.2 (A2,3,4,9)	+20.8 ± 2.3 (A2,3)
A 9	-52.2 ± 1.1 (A1,2,4,6,7,8,10,11)	-71.2 ± 1.8 (A1,2,4,6,7,8)	-61.1 ± 1.4 (A1,5,7,11)	-59.5 ± 3.2 (A1,4,6,7,8)	-8.7 ± 0.9 n.s.	+15.5 ± 0.9 (A8,10)	+28.5 ± 3.6 (A1,7,10)
A 10	-44.9 ± 1.2 (A1,2,4,5,6,7,9,11)	-66.3 ± 1.3 (A1,4,6,7,8)	-50.2 ± 2.2 (A1,5,7)	-54.9 ± 3.1 (A4)	-7.4 ± 0.91 (A6)	+5.6 ± 1.3 (A2,3,4,9)	+12.5 ± 1.0 (A2,3,5,6)
A 11	-35.6 ± 0.8 (A1,5,7,9,10)	-75.8 ± 4.2 (A1,2,3,4,6,7,8)	-49.4 ± 3.3 (A1,4,5,6,7,9)	-46.5 ± 1.8 (A3)	-8.3 ± 0.9 n.s.	+12.1 ± 2.3 (A3)	+19.4 ± 1.8 (A2,3,6)
p	<0.002	<0.002	<0.002	<0.002	<0.002	<0.002	<0.002

Note: Different accessions numbers are used to show significant differences under dehydration (treatment effect) from each other using mean values (±SE) over five replications at $p < 0.002$.

Abbreviations: A_n , net assimilation rate ($\mu\text{mol CO}_2 \text{ m}^{-2} \text{ s}^{-1}$); g_s , stomatal conductance ($\text{mol m}^{-2} \text{ s}^{-1}$); g_m , mesophyll conductance obtained from chlorophyll fluorescence method ($\text{mol CO}_2 \text{ m}^{-2} \text{ s}^{-1}$); Ψ_{leaflet} , leaflet water potential (MPa); L_{leaf} , leaf thickness (μm); θ_{IAS} , mesophyll porosity ($\text{m}^3 \text{ m}^{-3}$); g_{IAS} , intercellular airspace conductance ($\text{mol m}^{-2} \text{ s}^{-1} \text{ bar}^{-1}$).

TABLE 2 Pearson correlation coefficients between the absolute values

	Latitude (°N)	Temperature seasonality (CV)	Precipitation seasonality (CV)	Frost-free days
A_n	-0.728*	-0.541	0.447	0.553
g_m - fluorescence	-0.675	-0.475	0.311	0.538
θ_{IAS}	-0.603	-0.474	0.483	0.420
g_{IAS}	-0.712*	-0.435	0.856*	0.582
Leaf N	-0.603	-0.083	0.372	0.01

Note: Pearson correlation coefficients between the absolute values of the physiological and anatomical variables and climatic data for 11 *J. regia* accessions under dehydration treatment using mean values (\pm SE, $n = 5$). Bold indicates significance at $p < 0.05$ and * indicates significance after Bonferroni corrections ($p < 0.0025$).

Abbreviations: A_n , net assimilation; CV, coefficient of variation; IAS, intercellular airspace.

suggesting a potential positive impact of irrigation on leaf performance by improving CO_2 diffusion. The accessions with lower diffusion resistance (e.g., more porous leaves) benefit from a higher CO_2 diffusion capacity, and exhibit inherently higher performance and biochemical activities (i.e., V_{cmax}) under the common garden conditions of the experiment. Comparing $A - C_i$ and $A - C_c$ curves provides insights into the limitations imposed by mesophyll g_m on assimilation rate associated with the drawdown of CO_2 from IAS (C_i) to the chloroplast (C_c ; Figure 3). *J. regia* accessions from lower latitude exhibit enhanced performance through increasing V_{cmax} at low CO_2 concentrations, found by the net assimilation rate response to C_c ($A - C_c$ curve), when Rubisco is limiting A (Figure 3). That was in line with greater leaf nitrogen content for those accessions (Figure 4) and more investment toward Rubisco activity (Niinemets et al., 2009b; Sharkey et al., 2007; Warren & Adams, 2004), enhancing their A_n and CO_2 diffusion capacity at lower CO_2 concentrations (Figure 4). Greater maximum electron transport rate (J_{max}) also found using the $A - C_c$ curve, where RuBP- regeneration is limiting A , was associated with lower diffusion resistance through mesophyll (e.g., higher θ_{IAS}) and higher g_m , and higher enzymatic activity during CO_2 fixation and carbohydrate formation (i.e., Calvin cycle) for low latitude *J. regia* accessions. A_{max} was strongly associated to V_{cmax} and J_{max} (Figure S6), supporting greater biochemical and diffusional capacity for low latitude accessions which exhibit thicker leaves with greater θ_{IAS} and g_m , and more nitrogen accumulation within leaves.

On the other hand, the photosynthetic performance seems to be unrelated to the phylogenetic history. Accessions with greater A_n and A_{max} , such as A3 and A9, share a close evolutionary background with low-performance accessions, like A4 and A11, but not with each other (Figure 1B). Therefore, unlike studies that reported strong phylogenetic support for water stress resistant traits like xylem cavitation vulnerability in stem and root (Willson et al., 2008) or vein development, patterning and hydraulic conductance (Brodribb et al., 2007), our results suggest that geographical variability is more strongly linked with differences in photosynthetic rate in *Juglans* accessions. Therefore, high intraspecific variability in leaf anatomical characteristics and high variation in photosynthetic performance between *J. regia* accessions are in line with their establishment across

a wide range of habitats with contrasting environmental conditions. This is consistent with results of He et al. (2018b), who showed that species with lower variability in traits like specific leaf area have narrower habitat range, contrasting other studies with strong influence of phylogenetic history on traits variation (Homeier et al., 2021).

Leaf nitrogen content per unit area (Leaf N) was negatively related to latitude and supported higher A_n with greater biochemical activity. Increases in A_n related to changes in Leaf N and chlorophyll content have been reported for *Populus balsamifera* and *P. angustifolia* populations as an adaptive response to growing season length (Soolanayakanahally et al., 2009; Kaluthota et al., 2015). Latitudinal variation in photosynthetic variables have been reported more broadly across various species, however, the patterns were opposite in *Populus* spp. For example, latitudinal increases in A_n and for *P. trichocarpa* genotypes was accompanied by greater g_m through higher carbonic anhydrase activity and aquaporins functioning that were attributed to growth under shorter growing season in northern habitats (Gornall & Guy, 2007; McKown et al., 2014a, 2014b; Momayyezi & Guy, 2017, 2018).

4.3 | Dehydration-induced responses

As expected, dehydration negatively impacted photosynthesis in all accessions, but some exhibited greater reductions in A_n with decreases in g_m , g_s and $\Psi_{leaflet}$ ($p = 0.007$). Accessions A3, A5 and A9 exhibited similar absolute values to each other (Table S2) and had the highest photosynthetic capacity than other accessions, with the highest % reductions due to drought. A reduction in photosynthesis under dehydration was associated with decreases in PSII efficiency, which could be due to increases in photorespiration associated with increased resistance to CO_2 diffusion through stomata and mesophyll (Busch 2020; Neto et al., 2017; Sharkey 1988). Even under dehydration, accessions A3 and A5 from lower latitudes maintained A_n , g_m , θ_{IAS} , g_{IAS} and Leaf N higher than other accessions (Table 2), suggesting that these accessions hold potential for commercial production without increasing susceptibility to stress in absolute terms.

Dehydration reduced leaf thickness and increased θ_{IAS} and g_{IAS} by shrinking mesophyll cell size more than IAS (Table 1 and S2); this is consistent with our earlier observations for *J. regia* cv. Chandler and *J. microcarpa* (Momayyezi et al., 2022). In the current study, g_{IAS} increased by 13–35% in different *J. regia* accessions under dehydration. However, its contribution to g_m (calculated as described by Niinemets & Reichstein, 2003) was 7–23% under well-watered but decreased to 3–8% under drought across accessions, which is within the expected limiting range (3–37%) for woody perennial species with hypostomatous leaves (Harwood et al., 2021; Niinemets & Reichstein, 2003; Parkhurst & Mott, 1990; Tomás et al., 2013; Tosens et al., 2012). Additionally, reductions in the g_{IAS} contribution to g_m was closely and positively related to A_n ($R^2 = 0.63$; $p = 0.003$) and A_{max} ($R^2 = 0.37$; $p = 0.044$), suggesting reduced gas phase diffusion under stress may decrease photosynthesis further by limiting CO_2 diffusion in liquid phase through chloroplast re-positioning and activity of carbonic anhydrases and aquaporins (Evans et al., 2009; Miyazawa et al., 2008; Momayyezi et al., 2020; Tholen et al., 2008; Tomás et al., 2013).

4.4 | Conclusion

We found that photosynthetic capacity in *J. regia* accessions was associated with leaf anatomical and biochemical components that impact CO_2 diffusion. Leaves with greater porosity and g_{IAS} contribution to g_m exhibited the highest photosynthetic capacity at ambient and saturating CO_2 . Improved photosynthesis was supported by increased carboxylation capacity and leaf nitrogen accumulation. Higher photosynthesis across accessions was associated with frost-free days and precipitation and temperature seasonality patterns in low-latitude native habitats. Although *J. regia* has a limited resilience under dehydration, two of the low-latitude accessions (e.g. A3 and A5) with the highest inherent photosynthetic capacity, sustained performance under stress. These accessions hold promise for high productivity and use in breeding programs for commercial walnut production (Figure 2).

ACKNOWLEDGEMENTS

We are grateful to Chuck Fleck (Sierra Gold Nursery) for their help with the plant material selection and propagation. We thank the Stable Isotope Facility at UC Davis for the elemental analyses of the leaf samples. Mina Momayyezi was supported by a Katherine Esau Postdoctoral Fellowship funded by UC Davis. This study was funded by USDA-ARS CRIS funding (Research Project #5306-21220-004-00) and microCT beamtime was provided by the Advanced Light Source, which is supported by the Director, Office of Science, Office of Basic Energy Sciences, of the U.S. Department of Energy under Contract Number DE-AC02-05CH11231.

CONFLICT OF INTEREST

The authors declare no conflict of interest.

ORCID

Mina Momayyezi  <http://orcid.org/0000-0001-8039-3681>

Matthew E. Gilbert  <http://orcid.org/0000-0002-6761-7975>

Andrew J. McElrone  <http://orcid.org/0000-0001-9466-4761>

REFERENCES

- Baillie, A.L. & Fleming, A.J. (2020) The developmental relationship between stomata and mesophyll airspace. *New Phytologist*, 225, 1120–1126.
- Bernacchi, C.J., Portis, A.R., Nakano, H., von Caemmerer, S. & Long, S.P. (2002) Temperature response of mesophyll conductance; implications for the determination of rubisco enzyme kinetics and for limitations to photosynthesis in vivo. *Plant Physiology*, 130, 1992–1998.
- Bongi, G. & Loreto, F. (1989) Gas-exchange properties of salt-stressed olive (*Olea europaea* L.) leaves. *Plant Physiology*, 90, 1408–1416.
- Boyce, C.K., Brodribb, T.J., Feild, T.S. & Zwieniecki, M.A. (2009) Angiosperm leaf vein evolution was physiologically and environmentally transformative. *Proceedings of the Royal Society B*, 276, 1771–1776.
- Brodribb, T.J., Field, T.S. & Jordan, G.J. (2007) Leaf maximum photosynthetic rate and venation are linked by hydraulics. *Plant Physiology*, 144, 1890–1898.
- Buckley, T.N., John, G.P., Scoffoni, C. & Sack, L. (2017) The sites of evaporation within leaves. *Plant Physiology*, 173, 1763–1782.
- Busch, F.A. (2020) Photorespiration in the context of rubisco biochemistry, CO_2 diffusion and metabolism. *Plant Journal*, 101, 919–939.
- von Caemmerer, S. & Farquhar, G.D. (1981) Some relationships between the biochemistry of photosynthesis and the gas exchange of leaves. *Planta*, 153, 376–387.
- Davis, T.J., Gao, D., Gureyev, T.E., Stevenson, A.W. & Wilkins, S.W. (1995) Phase contrast imaging of weakly absorbing materials using hard x-rays. *Nature*, 373, 595–598.
- De Souza, A.P. & Long, S.P. (2018) Toward improving photosynthesis in cassava: characterizing photosynthetic limitations in four current African cultivars. *Food Energy Security*, 7, e00130.
- De Souza, A.P., Wang, Y., Orr, D.J., Carmo-Silva, E. & Long, S.P. (2020) Photosynthesis across African cassava germplasm is limited by rubisco and mesophyll conductance at steady state, but by stomatal conductance in fluctuating light. *New Phytologist*, 225, 2498–2512.
- Dowd, B.A., Campbell, G.H., Marr, R.B., Nagarkar, V.V., Tipnis, S.V. & Axe, L. et al. (1999) Developments in synchrotron X-ray computed microtomography at the National Synchrotron Light Source. In: U Bonse, ed. *SPIE's International Symposium on Optical Science, Engineering, and Instrumentation*. SPIE, pp. 224–236. Available from: <https://doi.org/10.1117/12.363725>
- Duke, J.A. (1978) The quest for tolerant germplasm. In: Jung, G.A. (Ed.) *Crop Tolerance to Suboptimal Land Conditions*. Wiley. <https://doi.org/10.2134/asapecpub32.c1>
- Earles, J.M., Buckley, T.N., Brodersen, C.R., Busch, F.A., Cano, F.J., Choat, B. et al. (2019) Embracing 3D complexity in leaf carbon–water exchange. *Trends in Plant Science*, 24, 15–24.
- Earles, J.M., Th eroux-Rancourt, G., Roddy, A.B., Gilbert, M.E., McElrone, A.J. & Brodersen, C.R. (2018) Beyond porosity: 3D leaf intercellular airspace traits that impact mesophyll conductance. *Plant Physiology*, 178, 148–162.
- Erickson, R.O. & Michelini, F.J. (1957) The plastochron index. *American Journal of Botany*, 44, 297–305.
- Evans, J.R. (2021) Mesophyll conductance: walls, membranes and spatial complexity. *New Phytologist*, 229, 1864–1876. Available from: <https://doi.org/10.1111/nph.16968>

- Evans, J.R., Kaldenhoff, R., Genty, B. & Terashima, I. (2009) Resistances along the CO₂ diffusion pathway inside leaves. *Journal of Experimental Botany*, **60**, 2235–2248.
- Faralli, M. & Lawson, T. (2020) Natural genetic variation in photosynthesis: an untapped resource to increase crop yield potential? *The Plant Journal*, **101**, 518–528.
- Fischer, R.A., Rees, D., Sayre, K.D., Lu, Z.M., Condon, A.G. & Saavedra, A.L. (1998) Wheat yield progress associated with higher stomatal conductance and photosynthetic rate, and cooler canopies. *Crop Science*, **38**, 1467–1475.
- Flexas, J., Barbour, M.M., Brendel, O., Cabrera, H.M., Carriquí, M., Díaz-Espejo, A. et al. (2012) Mesophyll diffusion conductance to CO₂: an unappreciated central player in photosynthesis. *Plant Science*, **193–194**, 70–84.
- Flexas, J., Díaz-Espejo, A., Berry, J.A., Cifre, J., Galmés, J. & Kaldenhoff, R. et al. (2007) Analysis of leakage in IRGA's leaf chambers of open gas exchange systems: quantification and its effects in photosynthesis parameterization. *Journal of Experimental Botany*, **58**, 1533–1543.
- Flexas, J., Ribas-Carbó, M., Diaz-Espezo, A., Galmés, J. & Medrano, H. (2008) Mesophyll conductance to CO₂: current knowledge and future prospect. *Plant Cell and Environment*, **31**, 602–621.
- Fulton, E., Rockwell, N. & Holbrook, M. (2017) Leaf hydraulic architecture and stomatal conductance: a functional perspective. *Plant Physiology*, **174**, 1996–2007.
- Genty, B., Briantais, J.M. & Baker, N.R. (1989) The relationship between the quantum yield of photosynthetic electron transport and quenching of chlorophyll fluorescence. *Biochimica et Biophysica Acta*, **990**, 87–92.
- Gilbert, M.E., Pou, A., Zwieniecki, M.A. & Holbrook, N.M. (2012) On measuring the response of mesophyll conductance to carbon dioxide with the variable J method. *Journal of Experimental Botany*, **63**, 413–425.
- Glaubitz, J.C., Casstevens, T.M., Lu, F., Harriman, J., Elshire, R.J., Sun, Q. et al. (2014) TASSEL-GBS: a high capacity genotyping by sequencing analysis pipeline. *PLoS One*, **9**, e90346. Available from: <https://doi.org/10.1371/journal.pone.0090346>
- Gornall, J.L. & Guy, R.D. (2007) Geographic variation in ecophysiological traits of black cottonwood (*Populus trichocarpa*). *Canadian Journal of Botany*, **85**, 1202–1213.
- Grant, J.A. & Shackel, K. (1998) Influence of irrigation water deficit on stem end kernel shrivel of Chandler walnuts. An annual research report submitted to the California Walnut Board. Available from: <https://ucanr.edu/sites/cawalnut/showyears/1998/?repository=66994&a=154103>
- Gürsoy, D., De Carlo, F., Xiao, X. & Jacobsen, C. (2014) TomoPy: a framework for the analysis of synchrotron tomographic data. *Journal of Synchrotron Radiation*, **21**, 1188–1193.
- Han, J., Lei, Z., Zhang, Y., Yi, X., Zhang, W. & Zhang, Y. (2019) Drought-introduced variability of mesophyll conductance in *Gossypium* and its relationship with leaf anatomy. *Physiologia Plantarum*, **166**, 873–887.
- Harley, P.C., Loreto, F., Di Marco, G. & Sharkey, T.D. (1992) Theoretical considerations when estimating the mesophyll conductance to CO₂ flux by analysis of the response of photosynthesis to CO₂. *Plant Physiology*, **98**, 1429–1436.
- Harrison, S., Spasojevic, M.J. & Li, D. (2020) Climate and plant community diversity in space and time. *Proceedings of the National Academy of Sciences of the United States of America*, **117**, 4464–4470.
- Harwood, R., Thérroux-Rancourt, G. & Barbour, M.M. (2021) Understanding airspace in leaves: 3D anatomy and directional tortuosity. *Plant, Cell & Environment*, **44**, 2455–2465. Available from: <https://doi.org/10.1111/pce.14079>
- He, D., Chen, Y., Zhao, K., Cornelissen, J.H.C. & Chu, C. (2018b) Intra- and interspecific trait variations reveal functional relationships between specific leaf area and soil niche within a subtropical forest. *Annals of Botany*, **12**, 1173–1182.
- He, N., Liu, C., Tian, M., Li, M., Yang, H., Yu, G. et al. (2018a) Variation in leaf anatomical traits from tropical to cold-temperate forests and linkage to ecosystem functions. *Functional Ecology*, **32**, 10–19.
- Hikosaka, K. & Shigeno, A. (2009) The role of rubisco and cell walls in the interspecific variation in photosynthetic capacity. *Oecologia*, **160**, 443–451.
- Homeier, J., Seeler, T., Pierick, K. & Leuschner, C. (2021) Leaf trait variation in species-rich tropical andean forests. *Scientific Reports*, **11**, 9993. Available from: <https://doi.org/10.1038/s41598-021-89190-8>
- Kaluthota, S., Pearce, D.W., Evans, L.M., Letts, M.G., Whitham, T.G. & Rood, S.B. (2015) Higher photosynthetic capacity from higher latitude: foliar characteristics and gas exchange of Southern, central and Northern populations of *Populus angustifolia*. *Tree Physiology*, **35**, 936–948.
- Kattge, J., Díaz, S., Lavorel, S., Prentice, I.C., Leadley, P., Bönsch, G. et al. (2011) TRY—a global database of plant traits. *Global Change Biology*, **17**, 2905–2935.
- Kluepfel, D., Leslie, C., Aradhya, M., Browne, G. et al. (2015) *Development of disease-resistant walnut root stocks: Integration of conventional and genomic approaches*. Walnut Research Reports. pp. 87–91. Available from: <http://ucanr.edu/repositoryfiles/2015-087-160265.pdf>
- Knipfer, T., Reyes, C., Momayyezi, M., Brown, P.J., Kluepfel, D. & McElrone, A.J. (2020) A comparative study on physiological responses to drought in walnut genotypes (RX1, vlach, VX211) commercially available as rootstocks. *Trees*, **34**, 665–678.
- Kruger, E.L. & Volin, J.C. (2006) Reexamining the empirical relation between plant growth and leaf photosynthesis. *Functional Plant Biology*, **33**, 421–429.
- Lampinen, B., Hasey, J., Metcalf, S. & Negrón, C. (2005) Irrigation management as a tool to stabilize and revitalize a declining 'chandler' orchard. An annual research report submitted to the California Walnut Board for 2005. Available from: <https://ucanr.edu/sites/cawalnut/AuthorsMR/MetcalfS/?repository=70834&a=154390>
- Legland, D., Arganda-Carreras, I. & Andrey, P. (2016) MorphoLibJ: integrated library and plugins for mathematical morphology with ImageJ. *Bioinformatics*, **32**, 3532–3534.
- Lehmeier, C., Pajor, R., Lundgren, M.R., Mathers, A., Sloan, J., Bauch, M. et al. (2017) Cell density and airspace patterning in the leaf can be manipulated to increase leaf photosynthetic capacity. *The Plant Journal*, **92**, 981–994.
- Leslie, C., McGranahan, G., Hackett, W., Martinez-Garcia, P.J., Wang, G., Ramasamy, R. et al. (2015) Walnut Improvement Program 2015. Available from: https://ucanr.edu/sites/cawalnut/category/genetic_breeding/
- Leslie, C.A. & McGranahan, G.H. (1998) The origin of the walnut. In: Ramos, D.E. (Ed.) *Walnut Production Manual*. Publication 3373. University of California. Division of Agriculture and Natural Resources, pp. 3–7. 319.
- Li, X., Blackman, C.J., Choat, B., Duursma, R.A., Rymer, P.D., Medlyn, B.E. et al. (2018) Tree hydraulic traits are coordinated and strongly linked to climate-of-origin across a rainfall gradient. *Plant, Cell and Environment*, **41**, 646–660.
- Long, S.P., Bernacchi, C.J. (2003) Gas exchange measurements, what can they tell us about the underlying limitations to photosynthesis? Procedures and sources of error. *Journal of Experimental Botany*, **54**, 2393–2401.
- Long, S.P., Zhu, X.G., Naidu, S.L. & Ort, D.R. (2006) Can improvement in photosynthesis increase crop yields? *Plant, Cell and Environment*, **29**, 315–330.
- Lundgren, M.R., Fleming, A.J. (2020) Cellular perspectives for improving mesophyll conductance. *The Plant Journal*, **101**, 845–857.
- Lundgren, M.R., Mathers, A., Baillie, A.L., Dunn, J., Wilson, M.J., Hunt, L. et al. (2019) Mesophyll porosity is modulated by the presence of functional stomata. *Nature Communications*, **10**, 2825. Available from: <https://doi.org/10.1038/s41467-019-10826-5>

- Marrano, A., Britton, M., Zaini, P.A., Zimin, A.V., Workman, R.E. & Puiu, D. et al. (2020) High-quality chromosome-scale assembly of the walnut (*Juglans regia* L.) reference genome. *GigaScience*, 9(5), g1aa050. <https://doi.org/10.1093/gigascience/g1aa050>
- McGranahan, G.H. & Leslie, C.A. (2009) Breeding walnuts (*Juglans regia*). In: Jain, S.M. & Priyadarshan, P.M. (Eds.) *Breeding plantation tree crops: temperate species*. New York, NY: Springer, pp. 249–273.
- McKown, A.D., Guy, R.D., Klápště, J., Galdes, A., Friedmann, M., Cronk, Q.C.B. et al. (2014a) Geographical and environmental gradients shape phenotypic trait variation and genetic structure in *Populus trichocarpa*. *New Phytologist*, 201, 1263–1276.
- McKown, A.D., Guy, R.D., Quamme, L.A., Klápště, J., La Mantia, J., Constabel, C.P. et al. (2014b) Association genetics, geography and ecophysiology link stomatal patterning in *Populus trichocarpa* with carbon gain and disease resistance trade-offs. *Molecular Ecology*, 23, 5771–5790.
- Miyazawa, S., Yoshimura, S., Shinzaki, Y., Maeshima, M. & Miyake, C. (2008) Deactivation of aquaporins decreases internal conductance to CO₂ diffusion in tobacco leaves grown under long-term drought. *Functional Plant Biology*, 35, 553–564.
- Momayyezi, M., Borsuk, A.M., Brodersen, C.R., Gilbert, M.E., Thérroux-Rancourt, G. & Kluepfel, D.A. (2022) Desiccation of the leaf mesophyll and its implications for CO₂ diffusion and light processing. *Plant, Cell & Environment*, 45, 1362–1381.
- Momayyezi, M. & Guy, R.D. (2017) Substantial role for carbonic anhydrase in latitudinal variation in mesophyll conductance of *Populus trichocarpa* Torr. & Gray. *Plant, Cell and Environment*, 40, 138–149.
- Momayyezi, M. & Guy, R.D. (2018) Concomitant effects of mercuric chloride on mesophyll conductance and carbonic anhydrase activity in *Populus trichocarpa* Torr. & Gray. *Trees*, 32, 301–309.
- Momayyezi, M., McKown, A.D., Bell, S.C.S. & Guy, R.D. (2020) Emerging roles for carbonic anhydrase in mesophyll conductance and photosynthesis. *The Plant Journal*, 101, 831–844.
- Moore, C.E., Meacham-Hensold, K., Lemonnier, P., Slattery, R.A., Benjamin, C., Bernacchi, C.J. et al. (2021) The effect of increasing temperature on crop photosynthesis: from enzymes to ecosystems. *Journal of Experimental Botany*, 72, 2822–2844.
- Muir, C.D., Conesa, M.À., Roldán, E.J., Molins, A. & Galmés, J. (2017) Weak coordination between leaf structure and function among closely related tomato species. *New Phytologist*, 213, 1642–1653.
- Neto, M.C.L., Cerqueira, J.V.A., da Cunha, J.R., Ribeiro, R.V. & Silveira, J.A.G. (2017) Cyclic electron flow, NPQ and photorespiration are crucial for the establishment of young plants of *Ricinus communis* and *Jatropha curcas* exposed to drought. *Plant Biology*, 19, 650–659.
- Niinemets, Ü. (1999) Research review. components of leaf dry mass per area thickness and density alter leaf photosynthetic capacity in reverse directions in woody plants. *New Phytologist*, 144, 35–47.
- Niinemets, Ü., Díaz-Espejo, A., Flexas, J., Galmés, J. & Warren, C.R. (2009b) Role of mesophyll diffusion conductance in constraining potential photosynthetic productivity in the field. *Journal of Experimental Botany*, 60, 2249–2270.
- Niinemets, Ü. & Reichstein, M. (2003) Controls on the emission of plant volatiles through stomata: a sensitivity analysis. *Journal of Geophysical Research*, 108, 4211. Available from: <https://doi.org/10.1029/2002JD002620>
- Niinemets, U., Wright, I.J. & Evans, J.R. (2009a) Leaf mesophyll diffusion conductance in 35 Australian sclerophylls covering a broad range of foliage structural and physiological variation. *Journal of Experimental Botany*, 60, 2433–2449.
- O'Donnell, M.S. & Ignizio, D.A. (2012) Bioclimatic predictors for supporting ecological applications in the conterminous United States. *U.S. Geological Survey Data Series*, 691, 10.
- Ordóñez, A. & Svenning, J.C. (2017) Consistent role of quaternary climate change in shaping current plant functional diversity patterns across european plant orders. *Scientific Reports*, 7, 42988. Available from: <https://doi.org/10.1038/srep42988>
- Parkhurst, D.F. & Mott, K.A. (1990) Intercellular diffusion limits to CO₂ uptake in leaves: studies in air and helox. *Plant Physiology*, 94, 1024–1032.
- Pearce, D.W., Millard, S., Bray, D.F. & Rood, S.B. (2006) Stomatal characteristics of riparian poplar species in a semi-arid environment. *Tree Physiology*, 26, 211–218.
- Peguero-Pina, J.J., Sisó S., Flexas, J., Niinemets, Ü, Sancho-Knapik, D. & Gil-Pelegrín E. (2017) Coordinated modifications in mesophyll conductance, photosynthetic potentials and leaf nitrogen contribute to explain the large variation in foliage net assimilation rates across *Quercus ilex* provenances. *Tree Physiology*, 37, 1084–1094.
- R Core Team (2017) R: *Alanguage and environment for statistical computing*. <https://www.R-project.org/>
- Reich, P.B. (2014) The world-wide 'fast-slow' plant economics spectrum: a traits manifesto. *Journal of Ecology*, 102, 275–301.
- Rosati, A., Metcalf, S., Buchner, R., Fulton, A. & Lampinen, B. (2006) Tree water status and gas exchange in walnut under drought, high temperature and vapour pressure deficit. *The Journal of Horticultural Science and Biotechnology*, 81(3), 415–420. Available from: <https://doi.org/10.1080/14620316.2006.11512082>
- Ruiz-Vera, U.M., Siebers, M.H., Jaiswal, D., Ort, D.R. & Bernacchi, C.J. (2018) Canopy warming accelerates development in soybean and maize, offsetting the delay in soybean reproductive development by elevated CO₂ concentrations. *Plant, Cell & Environment*, 41, 2806–2820.
- Salk, C. (2012) Within-species leaf trait variation and ecological flexibility in resprouting tropical trees. *Journal of Tropical Ecology*, 28, 527–530.
- SAS. (2013) *Statistical analysis software. Users' guide statistics version 9.4*. SAS Institute Inc., Cary.
- Schliep, K., Potts, A.J., Morrison, D.A. & Grimm, G.W. (2017) Intertwining phylogenetic trees and networks. *Methods in Ecology and Evolution*, 8, 1212–1220.
- Scoffoni, C., Vuong, C., Diep, S., Cochard, H. & Sack, L. (2014) Leaf shrinkage with dehydration: coordination with hydraulic vulnerability and drought tolerance. *Plant Physiology*, 164, 1772–1788.
- Sharkey, T.D. (1988) Estimating the rate of photorespiration in leaves. *Physiologia Plantarum*, 73, 147–152.
- Sharkey, T.D. (2016) What gas exchange data can tell us about photosynthesis. *Plant, Cell & Environment*, 39, 1161–1163.
- Sharkey, T.D., Bernacchi, C.J., Farquhar, G.D. & Singaas, E.L. (2007) Fitting photosynthetic carbon dioxide response curves for C₃ leaves. *Plant, Cell & Environment*, 30, 1035–1040.
- Simkin, A.J., López-Calcano, P.E. & Raines, C.A. (2019) Feeding the world: improving photosynthetic efficiency for sustainable crop production. *Journal of Experimental Botany*, 70, 1119–1140.
- Soolanayakanahally, R.Y., Guy, R.D., Slim, S.N., Drewes, E.C. & Schroeder, W.R. (2009) Enhanced assimilation rate and water use efficiency with latitude through increased photosynthetic capacity and internal conductance in balsam poplar (*Populus balsamifera* L.). *Plant, Cell and Environment*, 32, 1821–1823.
- Syvrtsen, J.P., Lloyd, J., McConchie, C., Kriedemann, P.E. & Farquhar, G.D. (1995) On the relationship between leaf anatomy and CO₂ diffusion through the mesophyll of hypostomatous leaves. *Plant, Cell and Environment*, 18, 149–157.
- Terashima, I., Hanba, Y.T., Tazoe, Y., Vyas, P. & Yano, S. (2006) Irradiance and phenotype: comparative eco-development of sun and shade leaves in relation to photosynthetic CO₂ diffusion. *Journal of Experimental Botany*, 57, 343–354.
- Thérroux-Rancourt, G., Earles, J.M., Gilbert, M.E., Zwieniecki, M.J., Boyce, C.K., McElrone, A.J. et al. (2017) The bias of a two-dimensional view: comparing two-dimensional and three-dimensional mesophyll surface

- area estimates using noninvasive imaging. *New Phytologist*, 215, 1609–1622.
- Théroux-Rancourt, G. & Gilbert, M.E. (2017) The light response of mesophyll conductance is controlled by structure across leaf profiles. *Plant, Cell and Environment*, 40, 726–740.
- Theroux-Rancourt, G., Jenkins, M.R., Brodersen, C.R., McElrone, A., Forrestel, E.J. & Earles, J.M. (2020) Digitally deconstructing leaves in 3D using x-ray microcomputed tomography and machine learning. *Applications in Plant Sciences*, 8, e11380.
- Tholen, D., Boom, C., Noguchi, K., Ueda, S., Katase, T. & Terashima, I. (2008) The chloroplast avoidance response decreases internal conductance to CO₂ diffusion in *Arabidopsis thaliana* leaves. *Plant, Cell and Environment*, 31, 1688–1700.
- Tomás, M., Flexas, J., Copolovici, L., Galmés, J., Hallik, L., Medrano, H. et al. (2013) Importance of leaf anatomy in determining mesophyll diffusion conductance to CO₂ across species: quantitative limitations and scaling up by models. *Journal of Experimental Botany*, 64, 2269–2281.
- Tosens, T. & Laanisto, L. (2018) Mesophyll conductance and accurate photosynthetic carbon gain calculations. *Journal of Experimental Botany*, 69, 5315–5318.
- Tosens, T., Niinemets, Ü., Vislap, V., Eichelmann, H. & Castro-Díez, P. (2012) Developmental changes in mesophyll diffusion conductance and photosynthetic capacity under different light and water availabilities in *Populus tremula*: how structure constrains function. *Plant, Cell & Environment*, 35, 839–856.
- Trueba, S., Théroux-Rancourt, G., Earles, J.M., Buckley, T.N., Love, D., Johnson, D.M. et al. (2022) The 3D construction of leaves is coordinated with water use efficiency in conifers. *New Phytologist*, 233, 851–861.
- USDA-NASS. (2020) 2019 California Walnut Acreage Report. https://www.nass.usda.gov/Statistics_by_State/California/Publications/Specialty_and_Other_Releases/Walnut/Acreage/2020walac_revised.pdf
- Warren, C.R. & Adams, M.A. (2004) What determines rates of photosynthesis per unit nitrogen in *Eucalyptus* seedlings? *Functional Plant Biology*, 31, 1169–1178.
- Williams, L.E. & Araujo, F. (2002) Correlations among predawn leaf, midday leaf, and midday stem water potential and their correlations with other measures of soil and plant water status in *Vitis vinifera* L. *Journal of the American Society for Horticultural Sciences*, 127, 448–454.
- Willson, C.J., Manos, P.S. & Jackson, R.B. (2008) Hydraulic traits are influenced by phylogenetic history in the drought-resistant, invasive genus *Juniperus* (Cupressaceae). *American Journal of Botany*, 95, 299–314.
- Wright, I.J., Reich, P.B., Westoby, M., Ackerly, D.D., Baruch, Z., Bongers, F. et al. (2004) The worldwide leaf economics spectrum. *Nature*, 428, 821–827.
- Zwieniecki, M.A., Brodribb, T.J. & Holbrook, N.M. (2007) Hydraulic design of leaves: insights from rehydration kinetics. *Plant, Cell and Environment*, 30, 910–921.

SUPPORTING INFORMATION

Additional supporting information can be found online in the Supporting Information section at the end of this article.

How to cite this article: Momayyezi, M., Rippner, D.A., Duong, F.V., Raja, P.V., Brown, P.J., Kluepfel, D.A., et al. (2022) Structural and functional leaf diversity lead to variability in photosynthetic capacity across a range of *Juglans regia* genotypes. *Plant, Cell & Environment*, 45, 2351–2365. <https://doi.org/10.1111/pce.14370>